Fast Dynamics of Type I ELM and Transport of ELM Pulse in JT-60U

N. Oyama, Y. Miura, A. V. Chankin, N. Asakura, K. Itami, T. Oikawa, H. Takenaga, M. Sugihara, Y. Kamada, K. Shinohara and the JT-60 Team

Japan Atomic Energy Research Institute, Naka-machi, Naka-gun, Ibarali 311-0193, Japan

e-mail contact of main author: oyaman@fusion.naka.jaeri.go.jp

Abstract. Simultaneous fast ELM measurements using reflectometer, interferometers, D_α intensity and magnetic probe reveal the detailed characteristics of type I ELMs. From the phase signal of the reflectometer indicating the radial movement of the cut-off layer, four different phases in an ELM event and radial extent of the collapse of density pedestal up to twice the pedestal width were observed. Detailed edge density measurements at high- and low-field side consistently demonstrate the asymmetry of collapse of density pedestal due to type I ELM, which is localized at the low-field side (LFS) midplane. Expelled particles from LFS midplane were measured by using LFS midplane and X-point Mach probes together with IRTV. Time delay of the enhanced ion saturation current between the two probes, and time constant of the peak heat load and the enhancement of the plasma flow toward divertor target suggest that the convective plasma flow provides large contribution to the ELM heat load.

1. Introduction

The study of the collapse of the pedestal structure due to type I ELMs [1-3] is important to clarify its mechanism and to reduce its severe heat loads on the divertor target, which can erode the divertor target plate in the next step devices such as ITER [4]. Therefore, the mitigation of the large ELM heat load on the divertor target is one of the most important issues to be overcome on ITER [5]. Since the ELM heat load strikes the divertor target not as a time-averaged load but as an instantaneous heat pulse, not only the evaluation of ELM energy but also the time scale of the collapse and transport from the viewpoint of individual ELM pulse is very important. In JT-60U, the study of detailed dynamics of the collapse of the density pedestal [6] has been started using O-mode reflectometer [7]. Fast time series analysis established the characteristic time scale of MHD oscillation and D_α spike in different density regimes [8]. Expelled particles from the plasma have been measured using scrape-off layer (SOL) Mach probe and fast infrared TV camera (IRTV) [9]. These kinds of detailed ELM measurement can provide important information to develop theoretical models of ELMs. In this paper, we report the fast dynamics of type I ELM and transport of ELM pulse in the SOL region from the viewpoint of individual ELM pulse using effective diagnostics with high temporal resolution in JT-60U to provide better understanding of the type I ELM physics.

2. Fast Time Series Analysis During an ELM

The measurement of the collapse of the density pedestal due to type I ELMs was performed on high-β_p H-mode discharges [10] with the following plasma parameters: plasma current I_p = 1.8 MA, toroidal magnetic field B_T = 4.0 T, NBI heating power P_{NBI} = 22 MW, triangularity δ ~ 0.32, elongation κ ~ 1.6 and safety factor at 95% flux surface q_{95} ~ 3.9. Figure 1 shows the plasma configuration of the discharge together with the line of sight of some diagnostics relevant to this study.

The phase angle change of reflectometer signal, which implies the radial movement of the cut-off layer, suggests the existence of four different phases in an ELM event: a precursor phase, collapse phase, recovery phase and a relaxation phase, as shown in FIG. 2(a) and (f). At first, coherent density precursor, whose amplitude increased with time, was clearly observed before the onset of an ELM. The time scale of the precursor phase was 200–500 μs in the frequency range of 5-25 kHz. On the other hand, no magnetic precursor was observed so far as shown in FIG. 2(h). In the collapse phase, the cut-off layer moved inward (positive phase change) as a result of the collapse of the density pedestal within 100–350 μs. It is noted that two vertical interferometers exhibited only small

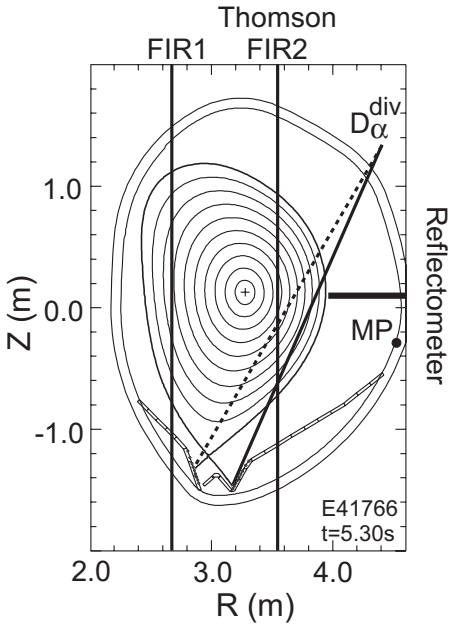

FIG. 1. Plasma configuration together with the line of sight of the FIR interferometer, Thomson scattering, D_α intensity at both divertor, the poloidal position of the magnetic probe (MP) and the reflectometer.

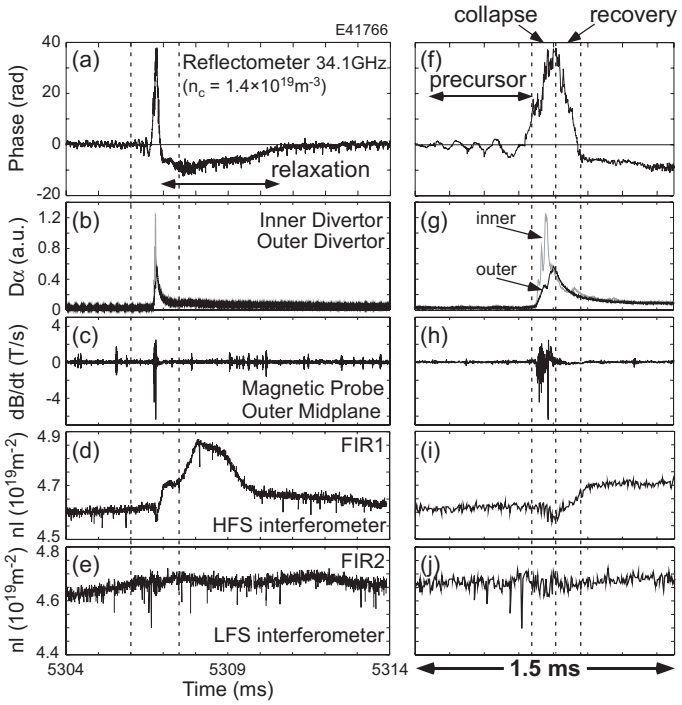

FIG. 2. Waveforms of (a) phase change of the reflectometer signal, (b) D_α intensity at inner (thin) and outer (thick) divertor, (c) magnetic fluctuation at outer midplae, (d) and (e) line-integrated density at high and low-field side, respectively. (f)-(j) show expanded waveforms between two dotted lines in (a)-(e) during 1.5s. Sampling time of the reflectometer, D_α intensity and magnetic probe is 1 μs. That of the interferometer is 5 μs. All diagnostics are synchronized within 5 μs.

oscillations in the collapse phase as shown in FIG. 2(i) and (j). Then, in the recovery phase, the cut-off layer moved outward as pedestal density first recovered and then went beyond the initial position over 200–500 μs. This overshoot resulted from the increase in the edge plasma density due to enhancement of divertor recycling and ionization as shown in FIG. 2(d). Finally, it gradually returned to a similar position as the initial one, taking 6–10 ms in the relaxation phase. The time scale of this relaxation phase is comparable to the time it takes the FIR1 signal to return to the initial level as shown in FIG. 2(a) and (d).

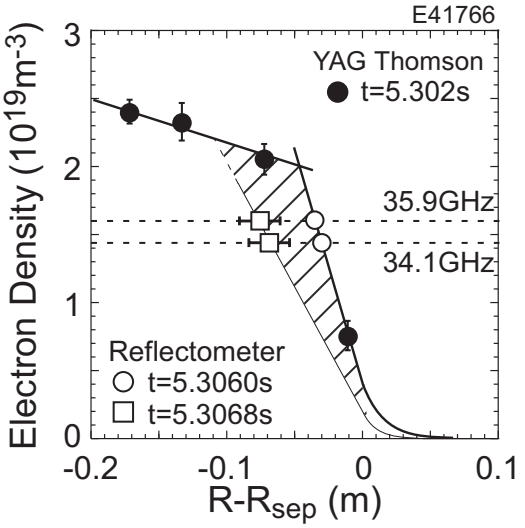

Fig. 3. Estimation of radial extent of the collapse. Open symbols show the cut-off position of the reflectometer. Thick (thin) line shows initial (assumed) density profile

The total phase change of the reflected signal, ϕ, under the WKB approximation is

$$\phi \cong \frac{2\omega}{c}\int_0^{x_c}\left(1-\frac{n(x)}{n_c}\right)^{1/2} dx - \frac{\pi}{2}, \qquad (1)$$

where n_c is the cut-off density, ω is the frequency of the incident wave and x_c is the distance from the antenna to the cut-off position. We can evaluate the radial movement of the cut-off layer using equation (1) and assuming possible density profiles satisfying the observed phase change. In the case of pedestal measurements in H-mode plasmas, the observed phase change is mainly attributed to the radial movement of the cut-off layer and to a smaller extent to changes in the density profile along the line of sight of the reflectometer. Figure 3 shows an example of estimation of radial movement of the cut-off layer for an ELM shown in FIG. 2. The cut-off position moved 7.5 cm inside the separatrix. This suggests that the radial extent of the collapse at the top of density pedestal reaches as large as twice the original pedestal width. The effect of the variation in the plasma equilibrium during ELMs was found to be less than 4 mm, which is 10 times smaller than estimated radial movement of the cut-off layer. For poloidally uniform density collapse, the number of lost particles by an ELM shown by the hutched region in FIG. 3 is estimated to be 1.0×10^{20}. Since the particle source during an ELM (~400 μs) was less than 2.0×10^{18}, this large particle loss should provide large reduction of FIR1 signal by $\delta nl \sim 0.48\times10^{19}$ m^{-2}. As mentioned above, however, no considerable reduction was observed during the collapse phase. This result suggests the asymmetry of the collapse of density pedestal by type I ELM.

3. Poloidal Asymmetry of Collapse of Density Pedestal by Type I ELM

In order to confirm the asymmetric collapse of pedestal structure due to type I ELM, three kinds of edge density measurements were performed. At first, simultaneous measurements of

edge density on the high-field side (HFS) and low-field side (LFS) plasma were performed using FIR1 and reflectometer, respectively, with the following plasma parameters: I_p = 1.0 MA, B_T = 2.0 T, P_{NBI} = 7.4 MW, $\delta \sim 0.35$, $\kappa \sim 1.4$ and $q_{95} \sim 2.9$. In this plasma configuration shown in FIG. 4(a), the line-integrated density on FIR1 is quite sensitive to the change of pedestal density, since half of the line of sight of FIR1 passed through the top of the density pedestal. The collapse of the density pedestal was manifested as fast inward movement of the cut-off layer at LFS midplane and the increase of D_α intensity at the timing shown by dotted line in FIG. 4(c). According to the estimation of radial extent from the phase change of the reflectometer shown in FIG. 4(b), the line-integrated density on FIR1 signal would be reduced by $\delta nl \sim 0.57\times10^{19}$ m^{-2}, if the collapse of density pedestal was a poloidally symmetric event. There was, however, no immediate response on FIR1 before the increase of D_α signal. Instead, the FIR1 signal usually showed a small reduction after about 90 μs average time delay. This time delay was comparable to the $L_{//}/C_s \sim 95$ μs, where $L_{//}$ is the connection length of ~ 25 m between LFS and HFS midplane, and C_s is the ion sound velocity of $\sim 2.8\times10^5$ m/s. Therefore, the delayed reduction can be explained by the parallel flow from the inside to outside in order to fill the density gap as a result of localized particle expulsion at LFS midplane.

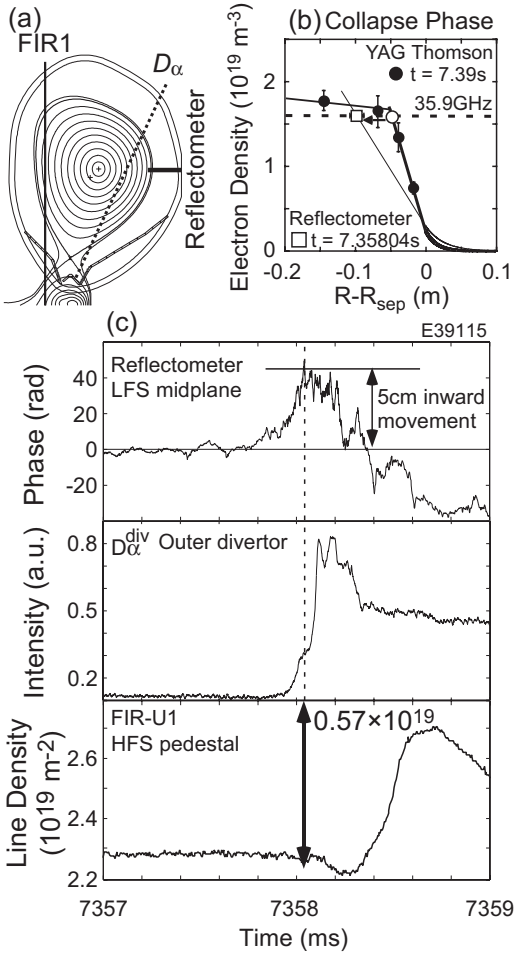

FIG. 4. (a) Plasma configuration. (b) Initial density profile (thick) and assumed density profile during collapse phase (thin). (c) Time evolution of phase change of reflectometer signal, D_α intensity and line-integrated electron density.

In order to confirm the absence of the direct particle loss corresponding to the collapse of the density pedestal at the HFS midplane, separatrix/SOL density measurement using

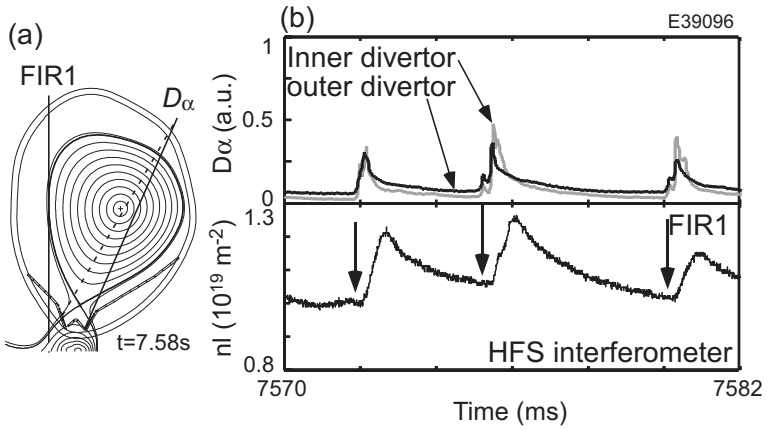

FIG. 5. (a) Plasma configuration together with the line of sight of FIR1. (b) Time evolution of FIR1 signal and D_α intensity at both divertor targets.

FIR1 was performed on the outward shifted plasma with the following plasma parameters: I_p = 1.2 MA, B_T = 2.5 T, P_{NBI} = 12.3 MW, $\delta \sim 0.40$, $\kappa \sim 1.3$ and $q_{95} \sim 3.0$. Since the integration length of separatrix/SOL region of FIR1 is about 0.7 m in this plasma configuration as shown in FIG. 5(a), such a small density increase of $\delta n_e = 0.5\times10^{18}$ m^{-3} should provide a detectable increase of $\delta nl \sim 3.7\times10^{17}$ m^{-2} prior to the increase of D_α signal. However, there was no density increase before the increase of D_α signal as shown in FIG. 5(b).

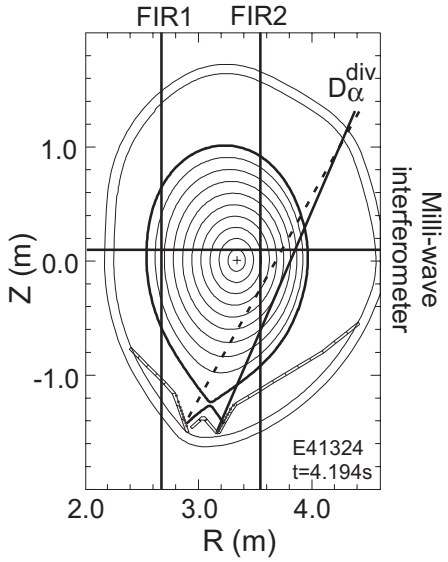

FIG. 6. Plasma configuration together with the line of sight of two vertical interferometers, millimeter-wave horizontal interferometer and D_α intensity at both divertor targets.

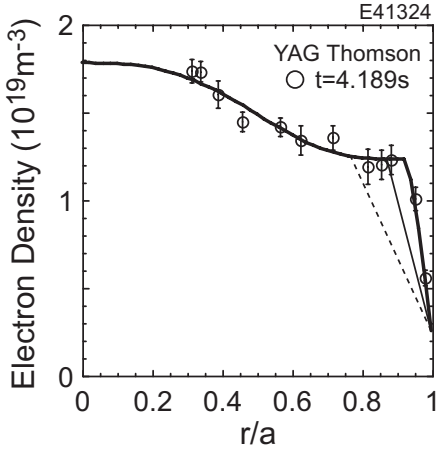

FIG. 8. Density profile before ELM (thick line). Estimated density profile to satisfy observed line-integrated density reduction on horizontal interferometer assuming linear density profile at pedestal region in two cases: poloidally uniform case (thin line) and only LFS case (dashed line).

Further evidence for the asymmetric collapse of density pedestal was obtained after a modification of the reflectometer system. When we change the polarization of the incident wave of the X-mode reflectometer [11], the system acts as a millimeter-wave interferometer (MWI) with the cut-off density of $n_c = 1.7\times10^{20}$ m^{-3}. In order to avoid the refraction by the plasma, the horizontal interferometer (MWI) was applied to relatively small plasma as shown in FIG. 6 with the following plasma parameters: I_p = 0.9 MA, B_T = 2.5 T, P_{NBI} = 7.1 MW, $\delta \sim 0.13$, $\kappa \sim$

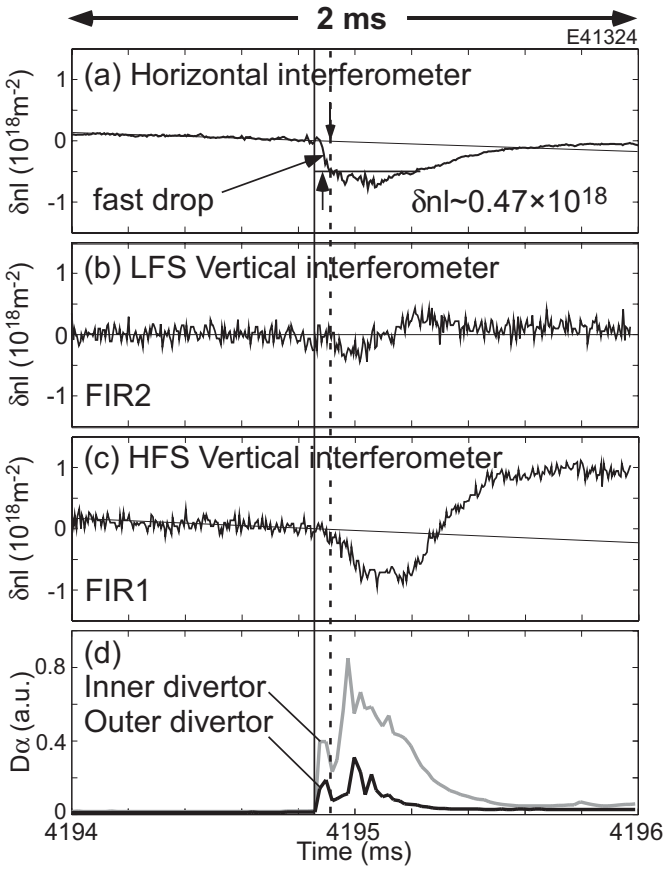

FIG. 7. Time evolution of (a)-(c) three interferometers and (d) D_α intensity at both divertor targets.

1.6 and q_{95} ~ 3.8. Figure 7 shows the time evolution of the line-integrated density of three interferometers together with D_α intensity at both divertor targets. Vertical solid line shows the onset of the ELM defined as the time of the increase in D_α intensity. At the time indicated by the dashed line, horizontal interferometer exhibited fast density loss of $\delta nl \sim 0.47\times10^{18}$ m^{-2}. Assuming poloidally uniform density loss with the profile shown by the thin solid line in FIG. 8 to satisfy the observed reduction of MWI signal, FIR1 signal should be reduced by $\delta nl \sim 2.8\times10^{18}$ m^{-2} (almost full range of FIG. 7(c)) at the timing shown by dashed line. However, no such fast drop was observed on both vertical interferometers as shown in FIG. 7 (b) and (c). Instead, the FIR1 signal showed a slow reduction 78 μs after the reduction of MWI signal, as in the previous experiment. This time delay was comparable to the transit time from LFS to HFS along the field line at the top of the density pedestal, $L_{//}/C_s \sim 80$ μs. Therefore, this reduction was also attributed to the parallel plasma flow toward the lost density region at LFS.

All these observations demonstrate consistently the poloidal asymmetry of the collapse of the density pedestal, which is localized at the low-field side midplane. The estimation of poloidal extent of the collapse of density pedestal as well as its radial extent is quite important to understand the mechanism of the collapse of pedestal structure. Although the direct measurement of the poloidal extent is difficult using the current diagnostics in JT-60U, we can evaluate the upper limit of the poloidal extent of the collapse. The average reduction of $\delta nl \sim 9.1\times10^{17}$ m^{-2} in FIR1 represents about 16 % of the expected reduction of $\delta nl \sim 5.7\times10^{18}$ m^{-2} obtained from the phase change of the reflectometer assuming poloidally uniform loss. Taking into account poloidal distribution of edge plasma volume enclosed between the flux surfaces, 16 % of edge plasma volume at LFS midplane corresponds to the poloidal angle of the collapse of the density pedestal of about ±40 degree.

4. Heat and particle transport of ELM pulse

Expelled particles from LFS midplane flow toward the divertor target along the magnetic field line. Such ELM pulse passing through the SOL region was studied by using two Mach probes at midplane and x-point, and divertor heat flux was measured with IRTV camera, as shown in FIG. 9. This kind of probe experiment was performed with the following plasma parameters: I_p = 1.0-1.1 MA, B_T = 2.0 T, P_{NBI} = 4.3-4.5 MW, $\delta \sim 0.34$, $\kappa \sim 1.3$ and $q_{95} \sim 3.8$. Figure 10 shows the time evolution of ion

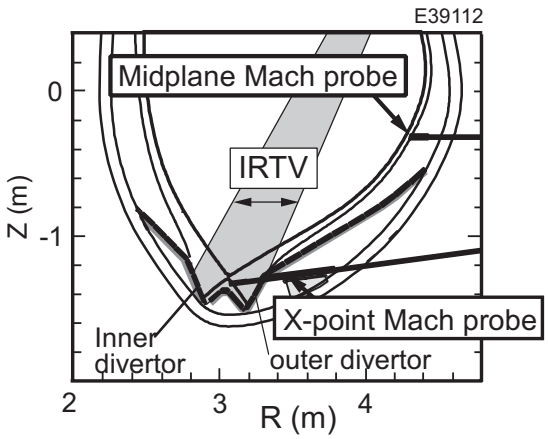

FIG. 9. Plasma configuration together with diagnostics arrangement of SOL probes and IRTV camera.

saturation currents at the upstream (j_s^{up}) and downstream (j_s^{down}) sides. At the onset of an ELM, abrupt increase of j_s was observed on the midplane probe. On the other hand, j_s in the x-point probe showed only gradual increase, with the peak value achieved 150 μs after the peak in the j_s of the midplane prove as shown in FIG. 10. Since this value is of the order of $L_{//}/C_s \sim 100$ μs, where $L_{//} \sim 26$ m and $C_s \sim 2.5\times10^5$ m/s evaluating from the pedestal plasma temperature, this time delay can be explained by the parallel convective flow of the expelled particles along the field line.

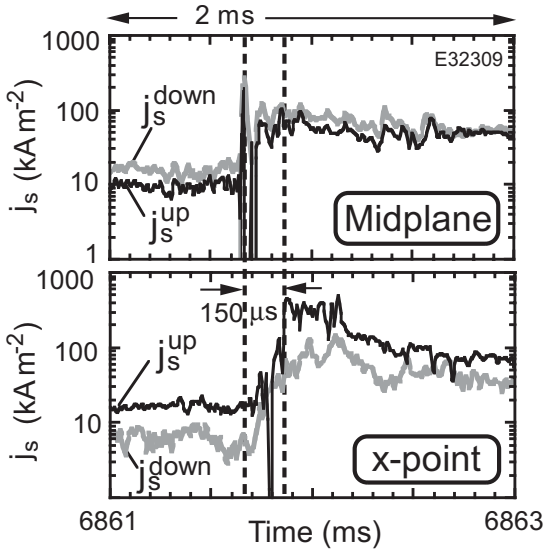

FIG. 10. Time evolution of ion-saturation current at the midplane (upper) and X-point

The time evolution of the heat flux at both divertor targets, j_s^{up} and stored energy is shown in FIG. 11. Duration of the peak heat flux corresponds to that of the enhancement of the plasma flow toward divertor. The fast drop of the stored energy by 19.3 kJ was also observed during the period of large heat flux deposition as shown by two dashed lines. The slow reduction of the stored energy in latter phase ($t > 5361$ ms) was attributed to the tail of the heat flux at the inner target as shown in FIG. 11(a). Summarizing these observations, the bulk of the heat load to the divertor targets may be carried by the parallel convective flow under these plasma conditions.

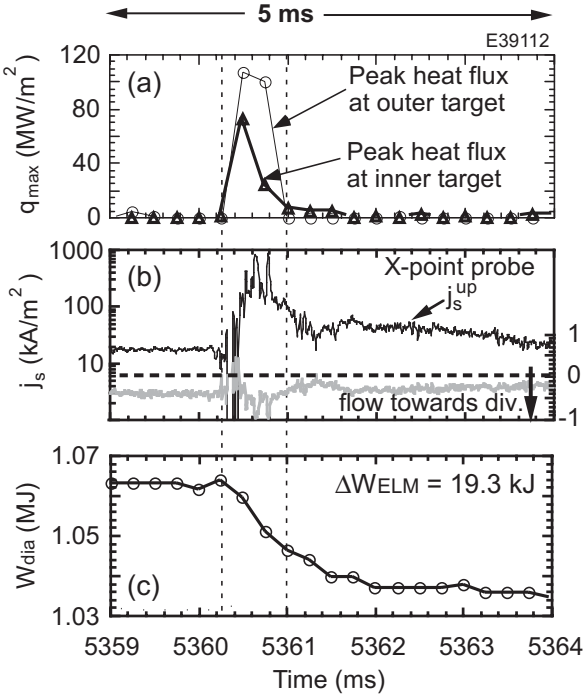

FIG. 11. Time evolution of (a) heat flux at both divertor target, (b) ion-saturation current of X-point probe and Mach number of the flow (gray) , and (c) stored energy.

5. Summary

Simultaneous fast ELM measurements using reflectometer, interferometers, D_α intensity and magnetic probe reveal the detailed characteristics of type I ELMs. From the phase signal of the reflectometer, an ELM event can be divided into a precursor phase, collapse phase, recovery phase and a relaxation phase. The typical time scale of each phase is 200-500 μs, 100-350 μs, 200-500 μs and 6-10 ms, respectively. The radial movement of the cut-off layer was estimated to be about 7.5 cm inside the separatrix during the collapse phase. The

following three kinds of edge density measurements consistently indicate that the collapse of the density pedestal during type I ELMs in JT-60U is localized at the low-field side midplane:

1. The collapse of the pedestal density was manifested as fast inward movement of the cut-off layer at the low-field side and the increase of D_α intensity. At this time, however, no considerable reduction was observed on high-field side interferometer.
2. No density increase corresponding to the direct particle loss from the high-field side midplane to the scrape-off layer was observed in SOL/separatrix density measurements.
3. Horizontal interferometer clearly exhibited fast density loss simultaneously with the increase of D_α intensity. However, no immediate response was observed on both high- and low-field side vertical interferometers.

Expelled particles from the LFS midplane were measured using LFS midplane and X-point Mach probes together with IRTV. Observed time delay between midplane and X-point probes was comparable to the parallel convective time between two probes, and the duration of the peak heat flux corresponds to that of the enhancement of the plasma flow toward divertor target. Therefore, the bulk of the heat load to the divertor targets may be carried by the parallel convective flow.

Acknowledgement

The authors acknowledge the members of the Japan Atomic Energy Research Institute who have contributed to the JT-60U projects.

Reference

[1] ZOHM, H., Plasma Phys. Control. Fusion **38** (1996) 105.
[2] CONNOR, J. W., Plasma Phys. Control. Fusion **40** (1998) 531.
[3] SUTTROP, W., Plasma Phys. Control. Fusion **42** (2000) A1.
[4] SHIMADA, M. et al., 2001 Fusion Energy 2000 (Proc. 18th Int. Conf. Sorrento, 2000) (Vienna: IAEA) CD-ROM file ITERP/05 and http://www.iaea.org/programmes/ripc/physics/fec2000/html/node1.htm
[5] G. Janeschitz, et al., J. Nucl. Mater. **290-293**, (2001) 1.
[6] OYAMA, et al., Plasma Phys. Control. Fusion **43** (2001) 717.
[7] OYAMA, N. and SHINOHARA, K., Rev. Sci. Instrum. **73** (2002) 1169.
[8] CHANKIN, A. V., et al., Nucl. Fusion **42** (2002) 733.
[9] ASAKURA, N, et al., Plasma Phys. Control. Fusion **44** (2002) A313.
[10] ISAYAMA, A, et al., this conference, EX/C2-2.
[11] SHINOHARA, K., et al., Rev. Sci. Instrum. **70** (1999) 4246.